Journal of Nuclear Materials 386–388 (2009) 82–85

Contents lists available at ScienceDirect

Journal of Nuclear Materials

journal homepage: www.elsevier.com/locate/jnucmat

Effects of porosity on the elastic behaviour of CVI SiC/SiC composites

L. Gélébart *, C. Colin

CEA Saclay, SRMA, BP49, 91191 cedex, Gif/Yvette, France

A B S T R A C T

The purpose of this paper is to deal with the effect of the complex geometry of the porosity of CVI SiC/SiC composites on the elastic behaviour at the scale of the tow, which is an intermediate scale before the modelling of the woven composite. For that purpose, the developed numerical approach consists in the generation of representative micro-structures and in a numerical periodic homogenization procedure for porous materials. As a result, the effective stiffness tensor of the tow is obtained. It will be useful in a further modelling at the upper scale (at scale of the woven composite the tow could be considered as homogeneous). In order to highlight the relevance of this approach, it is compared to a commonly used analytical Mori–Tanaka model. The anisotropy evaluated from the numerical approach is much higher than the anisotropy evaluated from the Mori–Tanaka model. Moreover, this numerical approach is able to evaluate the stress distribution within the composite and especially the high level of stress concentration induced by the complex geometry of the porosity. This high level of stress concentration will have to be taken into account when dealing with the initiation of damage within the composite.

1. Introduction

In the context of the development of fusion nuclear reactor, SiC/SiC composites are candidate for structural or functional applications at elevated temperature. A multi-scale approach is required to have a predictive modelling of their complex behaviour. The purpose of this paper focuses on the elastic behaviour of the composite at the scale of the tow (Fig. 1). CVI (chemical vapour infiltration) composites are studied and emphasis is put on the effect of the complex geometry of the porosity on the homogenized behaviour and on the local stress distribution.

2. Numerical homogenization procedure

2.1. Generation of representative CVI micro-structures

In this paper, the micro-structure is assumed to be invariant in the direction of the fibres and the cross-section is defined from a random distribution of fibres. The diameter of the fibres is assumed to be the same for all the fibres (7.5 μm which corresponds to TyrannoSA3 fibres) and a common volume fraction of fibres of 40% is used to generate a micro-structure of 150 fibres randomly distributed in a square area of $129 \times 129\ \mu m^2$. Five different distributions of fibres have been used.

For CVI composites, the process of SiC deposition on the fibres doesn't allow to fill completely the inter-fibres space so that a residual porosity with a complex geometry appears (Fig. 1 [1]). To represent the CVI process the infiltrated matrix is simulated by a layer of constant thickness of 3 μm at the surface of the fibres. The geometry of the porosity obtained with this representation is qualitatively in good agreement with the experimental observation (Figs. 1 and 2). The volume fractions of porosity obtained for the 5 distributions of fibres are quite similar (6.8%, 7.2%, 7.4%, 7.5% and 7.5%) with a mean value of 7.3% which is in good agreement with experimental measurements [2].

The procedure to generate and to mesh such random micro-structures has been developed with the free software *Salome* [3].

2.2. Material parameters

For the matrix, the local anisotropy induced by the local crystallographic texture of the SiC deposition [4] is neglected and the elastic behaviour is assumed to be isotropic with a Young modulus and a Poisson coefficient of 400 GPa and 0.18, respectively.

Fibres candidate for nuclear applications are Hi-Nicalon S or TyrannoSA3 fibres. The elastic properties of this last generation of SiC fibres are close to the properties of the matrix. The Young modulus (measured at CEA [5]), is 389 GPa and the Poisson coefficient is assumed to be 0.18.

2.3. Numerical modelling

In order to solve the elastic problem of periodic homogenization with a finite element code (*CAST3M* [6]), the geometry of the micro-structure described in Section 2.1, defined in a parallelepiped volume, has been meshed using linear prismatic elements

* Corresponding author.
E-mail address: Lionel.gelebart@cea.fr (L. Gélébart).

0022-3115/$ - see front matter © 2009 Elsevier B.V. All rights reserved.
doi:10.1016/j.jnucmat.2008.12.064

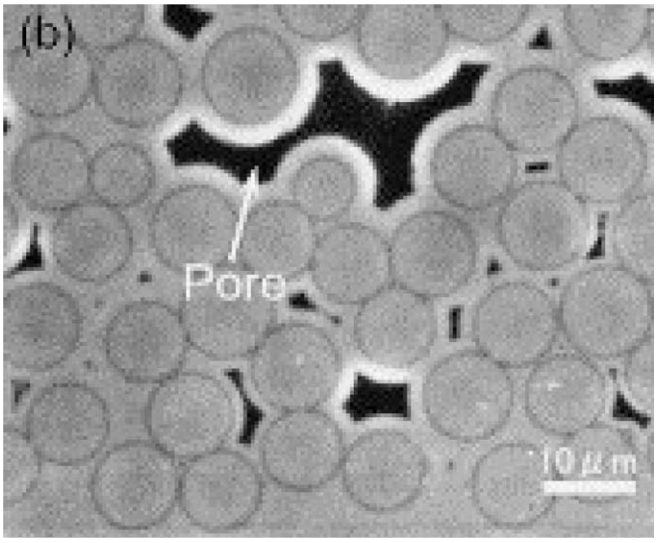

Fig. 1. Typical micro-structure of a CVI composite at the scale of the tow [1].

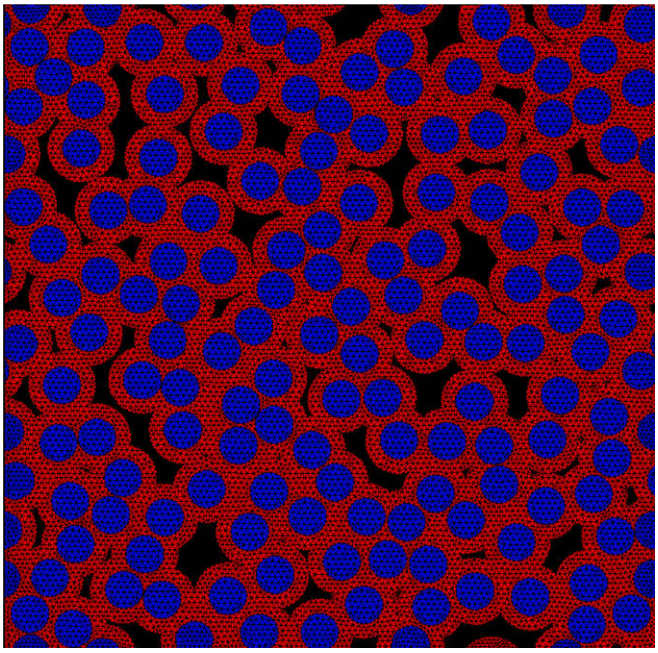

Fig. 2. Simulated micro-structure (due to the resolution of the picture, the mesh on the micro-structure is hard to see).

(6 nodes and 6 integration points), with one element in the thickness. The resulting mesh is periodic (i.e. each node on a surface has a corresponding node on the opposite surface). The set of differential equations used to solve this elastic problem are the classical volume equations added to specific boundary conditions.

2.3.1. Volume equations

For all points in the micro-structure, the stress tensor ($\underline{\underline{\sigma}}$) must satisfy the condition of local equilibrium (Eq. (1)), the stress and strain ($\underline{\underline{\varepsilon}}$) tensors are related by the 4th rank stiffness tensor K with the Hooke's law (Eq. (2)), and the displacement ($\underline{u}$) must satisfy the compatibility equation (Eq. (3)) (div and $grad$ are the classical divergence and gradient operators and $(K:\underline{\underline{\varepsilon}})_{ij} = \sum_{k,l} K_{ijkl}\varepsilon_{kl}$)

$$div(\underline{\underline{\sigma}}) = 0, \tag{1}$$

$$\underline{\underline{\sigma}} = K : \underline{\underline{\varepsilon}}, \tag{2}$$

$$\underline{\underline{\varepsilon}} = \frac{1}{2}(grad(\underline{u}) + grad^T(\underline{u})). \tag{3}$$

The resolution of the problem, numerically solved using a finite element method, consists in finding $\underline{\underline{\sigma}}$ and $\underline{u}$ for all points in the micro-structure satisfying Eqs. (1)–(3) and the following boundary conditions.

2.3.2. Periodic boundary conditions for porous materials

In order to apply a macroscopic stress tensor ($\underline{\underline{\Sigma}}$) with periodic conditions on this kind of porous micro-structure, the following boundary conditions have been implemented in the finite element code *CAST3M* [6].

The micro-structure is defined in a parallelepiped volume V with 6 planarsurfaces ($S_1, S_2, S_3, S_4, S_5, S_6$), S_i and S_{i+3} being opposite surfaces. Each surface S_i can be divided into two parts: the effective surface S_i^{eff} and the surface associated to the porosity S_i^{por}($S_i = S_i^{eff} \cup S_i^{por}$). To account for porosity, the normal stress $\underline{\underline{\sigma}}.\underline{n}_i$ on S_i^{eff} has to satisfy Eqs. (4) and (5), with $\underline{n}_i$ the outing normal at the surface S_i. As $\underline{\underline{\sigma}}.\underline{n}_i$ on S_i^{por} can be defined as a null vector, the average of $\underline{\underline{\sigma}}\underline{n}_i$ on the whole surface S_i is equal to $\underline{\underline{\Sigma}}\underline{n}_i$.

$$\underline{\underline{\sigma}}.\underline{n}_i = \alpha\underline{\underline{\Sigma}}.\underline{n}_i, \tag{4}$$

$$\alpha = \frac{\|S_i\|}{\|S_i^{eff}\|}. \tag{5}$$

Additional conditions are applied on 3 points of the micro-structure to avoid the rigid motion of the micro-structure (i.e. to ensure the unicity of the solution).

At this stage, the simulation can be performed. This set of conditions corresponds to Static Uniform Boundary Conditions [7]: the stress is uniform on each point of S_i^{eff} (see Eq. (4)).

Finally, the periodicity condition is satisfied if the difference of displacement between two corresponding points (M_i, M_{i+3}) in opposite surfaces (S_i^{eff}, S_{i+3}^{eff}) is constant (Eq. (6) with (M_i^*, M_{i+3}^*), two corresponding points arbitrary chosen in (S_i^{eff}, S_{i+3}^{eff})). Fig. 3 gives a schematic visualization of Eq. (6)

$$\underline{u}(M_i) - \underline{u}(M_{i+3}) = \underline{u}(M_i^*) - \underline{u}(M_{i+3}^*). \tag{6}$$

Numerically, these conditions (Eq. (6)) are satisfied through the introduction of Lagrange multipliers. As a consequence, the solution

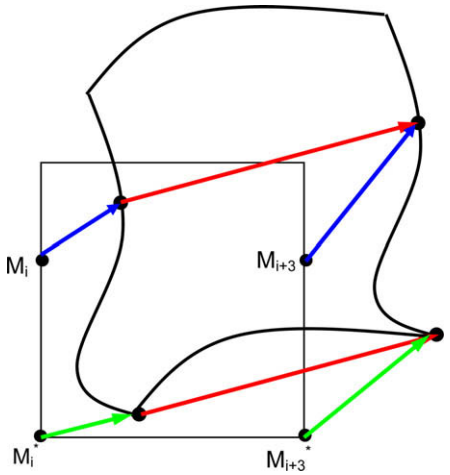

Fig. 3. Schematic visualization of the periodic boundary condition (the red vector is constant for all corresponding points in opposite surfaces, then $\underline{u}(M_i) - \underline{u}(M_{i+3}) = \underline{u}(M_i^*) - \underline{u}(M_{i+3}^*)$).

of the problem gives rise to reactions forces at each point (node) of S_i^{eff} so that the stress is no more uniform on S_i^{eff}.

2.3.3. Post-treatment: the effective behaviour

It can be demonstrated [8] (and it is numerically verified) that the mean stress on the whole micro-structure V (including porosity, where $\underline{\underline{\sigma}}$ is defined as a null tensor), $<\underline{\underline{\sigma}}>_V$, is equal to the macroscopic applied stress $\underline{\underline{\Sigma}}$ (Eq. (7))

$$<\underline{\underline{\sigma}}>_V = \underline{\underline{\Sigma}}. \tag{7}$$

On the other hand, the mean strain $<\underline{\underline{\varepsilon}}>_V$ has to be evaluated on the micro-structure but the strain cannot be evaluated within the porosity (i.e. the displacement field is not defined). As it is demonstrated [8] that Eq. (6) is equivalent to Eq. (8), the mean strain can be evaluated from the displacements of three couples of corresponding points (one couple per couple of opposite surfaces)

$$\underline{u}(M_i) - \underline{u}(M_{i+3}) = <\underline{\underline{\varepsilon}}>_V . \underline{M_i M_{i+3}}. \tag{8}$$

Finally, the effective stiffness tensor of the micro-structure $\tilde{K}$ (Eq. (9)) can be fully determined from six different simulations performed with six different applied stresses $\underline{\underline{\Sigma}}$

$$<\underline{\underline{\sigma}}>_V = \tilde{K} :<\varepsilon>_V. \tag{9}$$

The effective stiffness tensor presented in Section 3 is averaged on the results obtained for five different micro-structures.

3. Effect of porosity on the effective behaviour

In order to emphasize the relevance of this numerical approach, a classical analytical Mori–Tanaka model (see equations in [9]) is used assuming a simplified geometry of the porosity (circular cylinders with a volume fraction of 7.3%). In this calculation, the elastic heterogeneity between matrix and fibres (400 and 389 GPa) is reasonably neglected (the Young modulus is assumed to be equal to 395 GPa for both the matrix and the fibres). The effective stiffness tensors obtained with the finite element and the Mori–Tanaka models, $\tilde{K}^{FE}$ and $\tilde{K}^{MT}$, are given in Eq. (10). To visualize the anisotropy of the behaviour the evolution of the apparent elastic modulus as a function of the angle between the fibres and the tensile test direction is represented on Fig. 4

$$\tilde{K}^{FE} = \begin{pmatrix} 251.2 & 55.5 & 55.2 & 0 & 0 & 0 \\ 55.5 & 251.2 & 55.2 & 0 & 0 & 0 \\ 55.2 & 55.2 & 386.4 & 0 & 0 & 0 \\ 0 & 0 & 0 & 195.7 & 0 & 0 \\ 0 & 0 & 0 & 0 & 241.9 & 0 \\ 0 & 0 & 0 & 0 & 0 & 241.9 \end{pmatrix}$$

$$\tilde{K}^{MT} = \begin{pmatrix} 350.6 & 84.6 & 78.3 & 0 & 0 & 0 \\ 84.6 & 350.6 & 78.3 & 0 & 0 & 0 \\ 78.3 & 78.3 & 394.4 & 0 & 0 & 0 \\ 0 & 0 & 0 & 298.7 & 0 & 0 \\ 0 & 0 & 0 & 0 & 302.9 & 0 \\ 0 & 0 & 0 & 0 & 0 & 302.9 \end{pmatrix}. \tag{10}$$

When the tensile test direction is parallel to the direction of the fibres, the two models are consistent and the apparent Young modulus can be obtained with a classical mixture rule for a parallel assembly. In this direction, there is no effect of the geometry of the porosity.

On the contrary, when the tensile test direction is perpendicular to the direction of the fibres, the Mori–Tanaka model is much stiffer than the finite element model. This difference reveals that the complex shape of the porosity has to be taken into account through a numerical approach to obtain a good description of the elastic anisotropy of the composite.

4. Effect of porosity on the stress distribution

The numerical approach can be used to evaluate the full distribution of the local stresses which cannot be evaluated from analytical models.

4.1. Average stresses

The evolution of the normalized average tensile stresses (average tensile stress divided by the macroscopic tensile stress) within the fibres and the matrix is represented on Fig. 5 as a function of the tensile test direction. The main result is that the evolution of these average stresses is not significant compared to the evolution of the macroscopic behaviour (Section 3). As a consequence, a more detailed description of the stress distribution is required.

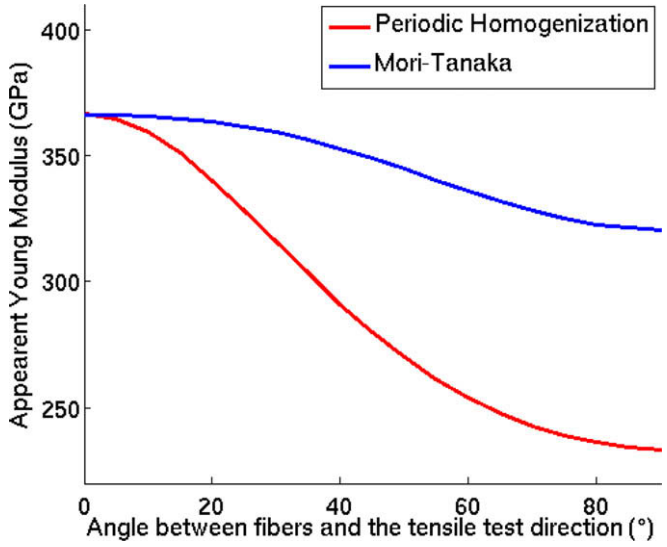

Fig. 4. Evolution of the apparent elastic modulus as a function of the tensile test direction.

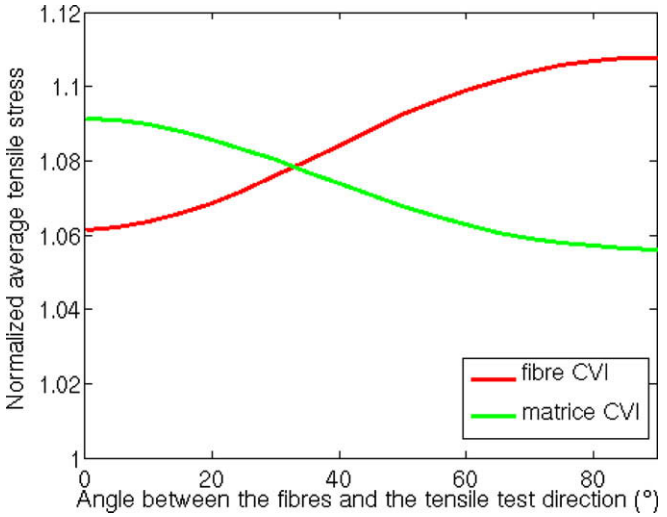

Fig. 5. Evolution of the normalized average tensile stress (average tensile stress/macroscopic tensile stress) within the fibres and the matrix as a function of the tensile test direction.

4.2. Stress heterogeneities

For a tensile test direction parallel to the direction of the fibres, the micro-structure can be regarded as a parallel assembly (with identical Poisson coefficients). Consequently, the stress field is uniaxial and homogeneous within the fibres and the matrix (the value of the stress in each constituent is equal to the average values given in Section 4.1).

For a tensile test direction perpendicular to the direction of the fibres, the statistical distributions of the local tensile stress (i.e. the stress in the direction of the tensile test) can be observed on Fig. 6.

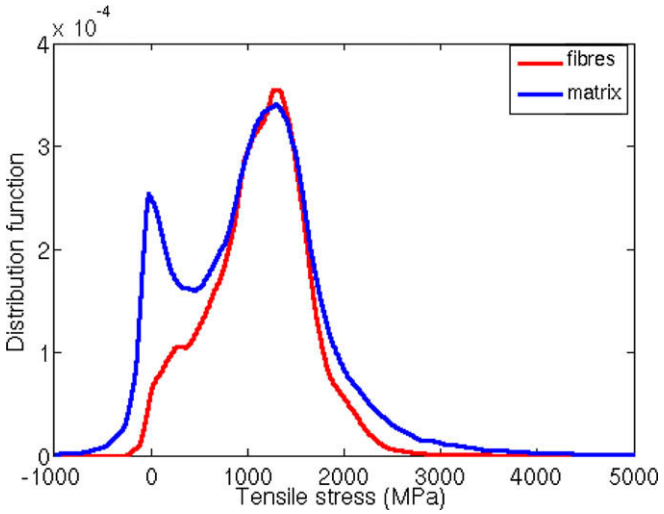

Fig. 6. Distribution of the tensile stress within the fibres and the matrix for a macroscopic tensile test (1 GPa) in the transverse direction.

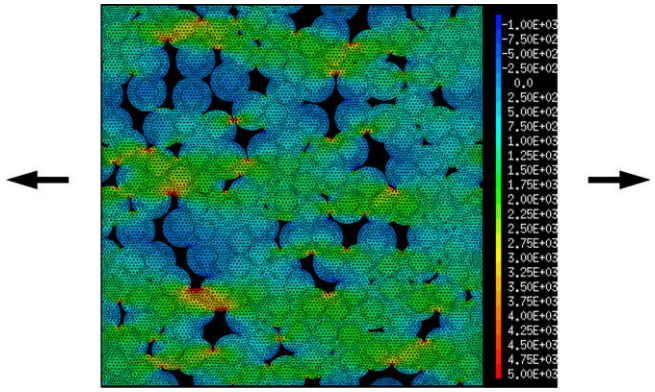

Fig. 7. Axial stress field for a macroscopic tensile test (1 GPa) in the transverse direction.

These distributions exhibit two clearly distinct peaks and large queues from −0.5 up to 4 times the macroscopic stress. This wide distribution is correlated to the spatial distribution of the stress: the porosity of CVI composites induces a high level of stress concentration but also a discharge of the stress in parts of the composite (Fig. 7).

The wider stress distribution in the matrix than in the fibres can be explained by the fact that the matrix is directly in contact with the porosity.

5. Conclusion

To account for the effect of the complex geometry of the porosity observed in CVI composites at the scale of the tow, a numerical homogenization procedure has been developed. This procedure consists in the generation of representative micro-structures and in a numerical periodic homogenization procedure for porous materials. This numerical approach is able to evaluate both the effective elastic behaviour of the tow and the stress heterogeneities within the tow.

As a result, the effective stiffness tensor of the tow $\tilde{K}$ (Section 3) is now available and can be used in a further modelling at the upper scale. At the scale of the woven composite, the tow could be regarded as homogeneous with the homogenized stiffness tensor $\tilde{K}$. The condition of scale separability, associated to the size of the representative volume element, will be discussed in a further work.

A comparison between this numerical approach and a classical Mori–Tanaka model reveals that the complex geometry of the porosity plays a significant role on the anisotropy of the effective behaviour.

Finally, such a numerical approach is able to evaluate the distribution of the local stresses within the composite. An important result is that the complex geometry of the porosity induces strongly heterogeneous stress distribution with a high level of stress concentration that will have to be taken into account when dealing with damage initiation especially in the matrix in which the stress distribution is the widest.

References

[1] N. Igawa, T. Taguchi, T. Nozawa, L.L. Snead, T. Hinoki, J.C. McLaughlin, Y. Katoh, S. Jitsukawa, A. Kohyama, J. Phys. Chem. 66 (2005) 551.
[2] Calard V, PhD Thesis, University of Bordeaux 1, 1998.
[3] <http://salome-plateforme.org>.
[4] D. Helary, O. Dugne, X. Bourrat, P.H. Jouneau, F. Cellier, J. Nucl. Mater. 350 (3) (2006) 332.
[5] L. Pierquet, L. Gélébart, T. Cozzika, S. Doriot, J. Pelé, F. Onimus, D. Hamon, L. Gosmain, H. Martin, P. Bonnaillie, CEA Internal Report, DMN/SRMA/LC2M/2006-2791/A, 2006.
[6] <http://www-cast3m.cea.fr>.
[7] T. Kanit, S. Forest, I. Galliet, V. Mounoury, D. Jeulin, Int. J. Solid Str. 40 (2003) 3647.
[8] M. Bornert, T. Bretheau, P. Gilormini, Hermes, ISBN 2-7462-0199-2, 2001.
[9] H. Huang, R. Taljera, Comp. Sci. Technol. 65 (2005) 1964.